# Cortical sources of Vernier acuity in the human visual system: An EEG-source imaging study

**Chuan Hou**
The Smith-Kettlewell Eye Research Institute, San Francisco, CA, USA
Department of Ophthalmology and Vision Research Laboratory, State Key Laboratory of Biotherapy, West China Hospital, Sichuan University, Chengdu, China

**Yee-Joon Kim**
The Smith-Kettlewell Eye Research Institute, San Francisco, CA, USA
Institute for Basic Sciences, Daejon, Korea

**Preeti Verghese**
The Smith-Kettlewell Eye Research Institute, San Francisco, CA, USA

**Vernier acuity determines the relative position of visual features with a precision better than the sampling resolution of cone receptors in the retina. Because Vernier displacement is thought to be mediated by orientation-tuned mechanisms, Vernier acuity is presumed to be processed in striate visual cortex (V1). However, there is considerable evidence suggesting that Vernier acuity is dependent not only on structures in V1 but also on processing in extrastriate cortical regions. Here we used functional magnetic resonance imaging–informed electroencephalogram source imaging to localize the cortical sources of Vernier acuity in observers with normal vision. We measured suprathreshold and near-threshold responses to Vernier onset/offset stimuli at different stages of the visual cortical hierarchy, including V1, hV4, lateral occipital cortex (LOC), and middle temporal cortex (hMT+). These responses were compared with responses to grating on/off stimuli, as well as to stimuli that control for lateral motion in the Vernier task. Our results show that all visual cortical regions of interest (ROIs) responded to both suprathreshold Vernier and grating stimuli. However, thresholds for Vernier displacement (Vernier acuity) were lowest in V1 and LOC compared with hV4 and hMT+, whereas all visual ROIs had identical thresholds for spatial frequency (grating acuity) and for relative motion. The cortical selectivity of sensitivity to Vernier displacement provides strong evidence that LOC, in addition to V1, is involved in Vernier acuity processing. The robust activation of LOC might be related to the sensitivity to the relative position of features, which is common to Vernier displacement and to some kinds of texture segmentation.**

Vernier acuity is a measure of the smallest positional offset of visual features with a precision better than the sampling resolution of the cone receptors in the retina (Westheimer, 1979). As such, it has been termed *hyperacuity*. The site of hyperacuity processing is presumed to be cortical (Klein & Levi, 1985; Levi, Klein, & Aitsebaomo, 1985; Norcia, Wesemann, & Manny, 1999; Skoczenski & Norcia, 2002; Victor & Conte, 2000; Westheimer & Hauske, 1975; Wilson, 1986), because the sensitivity to local position information exceeds the optical and photoreceptor sampling limits imposed by the eye (Geisler, 1984).

Oriented filters in striate cortex (V1) can explain many aspects of Vernier processing. Neurons in V1 are highly selective to the size and orientation of targets (Hubel & Wiesel, 1962; Shapley, Hawken, & Ringach, 2003). Many computational models of hyperacuity based on size and orientation filters assume that striate mechanisms critically limit the extraction of hyperacuity information (Duncan & Boynton, 2003; Klein & Levi, 1985; Watt & Morgan, 1985; Wilson, 1986). Psychophysical masking studies also suggest that striate mechanisms underlie Vernier acuity (Findlay, 1973; Levi, Klein, & Carney, 2000; Waugh, Levi, & Carney, 1993). Levi and colleagues (2000) reported that Vernier acuity depends strongly and nonmonotonically on spatial frequency with orientation dependence.

Citation: Hou, C., Kim, Y-J., & Verghese, P. (2017). Cortical sources of Vernier acuity in the human visual system: An EEG-source imaging study. *Journal of Vision*, *17*(6):2, 1–12, doi:10.1167/17.6.2.

doi: 10.1167/17.6.2 Received October 1, 2016; published June 2, 2017 ISSN 1534-7362 

However, there is also considerable evidence suggesting that detection of Vernier offsets may depend on cortical areas outside V1. Evidence of extrastriate involvement comes from the results of Srebro and Osetinsky (1987) who showed that electroencephalogram (EEG) activity evoked by Vernier offsets of extended line segments peaked at electrodes 6 cm lateral to Oz (the pole of occipital scalp area), suggesting extrastriate involvement. Similarly, Steinman and Levi (1992) found that Vernier and other spatial localization–related activity at electrode sites peaked at electrode locations outside of Oz. A functional magnetic resonance imaging (fMRI) study in humans found a distributed network of frontal, parietal, occipital, and cerebellar cortical areas that were selectively activated by Vernier offset stimuli (Sheth et al., 2007). Although these studies suggest that Vernier acuity may involve extrastriate mechanisms, further evidence is required to determine the specific extrastriate areas that are most sensitive to Vernier displacement.

Previous studies have shown that Vernier thresholds obtained from visual evoked potentials (VEP) match well with Vernier thresholds from psychophysics (Hou, Good, & Norcia, 2007; Levi, Manny, Klein, & Steinman, 1983; Steinman, Levi, Klein, & Manny, 1985; Zak & Berkley, 1986). Norcia and colleagues (1999) modified the original paradigm (Levi et al., 1983; Steinman et al., 1985; Zemon & Ratliff, 1982, 1984) to measure Vernier onset/offset thresholds with the steady-state VEP (SSVEP) by introducing a series of breaks in a square-wave luminance grating. Their results demonstrated that the first harmonic component measures the sensitivity to positional offset (Vernier acuity) and the second harmonic component measures the sensitivity to relative motion. In this study, we adapt the VEP paradigms for Vernier acuity from Norcia and colleagues (1999) and for grating acuity from Norcia and Tyler (1985) and use fMRI-informed EEG source imaging to localize the cortical sources of Vernier acuity and grating acuity in observers with normal vision.

Our approach here is to compare SSVEP measures of Vernier and grating acuity and their cortical loci, as these two acuities reflect different levels of neural processing. Grating acuity is thought to be limited strictly by retinal-striate factors, whereas Vernier acuity is further limited by cortical factors (Levi et al., 1985). Psychophysical studies have shown that amblyopia affects Vernier acuity more severely than grating acuity (Levi & Klein, 1982a, 1982b; McKee, Levi, & Movshon, 2003). Understanding what cortical areas are sensitive to Vernier acuity processing may shed light on the cortical pathways affected in amblyopia.

# Methods

## Participants

A total of 15 adult volunteers (eight male and seven female; age range, 28–62 years) enrolled in the study. All participants took part in the Vernier and lateral motion experiments, while 13 took part in the grating experiments. All participants had acuity equal to or better than 20/20 (Bailey–Lovie chart with five letters per line) with stereoacuity of at least 40 arcsec (random-dot stereo test, Stereo Optical Co., Inc., Chicago, IL). The research protocol was approved by the Institutional Review Board of The Smith-Kettlewell Eye Research Institute and conformed to the tenets of the Declaration of Helsinki. After the EEG recording and MRI scan procedures were explained, written informed consent was obtained before any testing.

## Visual stimuli

As illustrated in Figure 1, three protocols for Vernier, lateral motion, and grating sensitivity were conducted in the same SSVEP recording session. All stimuli alternated between two states at a rate of 3.75 Hz with a Michelson contrast of 90% with minimum and maximum luminance of 5 and 184.2 (cd/m$^2$), respectively. For each protocol, we conducted both a fixed and a swept SSVEP paradigm. For the fixed paradigm, suprathreshold displacement of 8 arcmin was used for both Vernier onset/offset and lateral motion conditions, and 3 cpd spatial frequency was used for the grating on/off condition. For the swept paradigm, the size of the displacements of Vernier offset ranged from 0.5 to 8 arcmin in 10 equal logarithmic steps over a period of 10 s, and the spatial frequency of gratings ranged from 2 to 30 cpd in 10 equal linear steps.

Visual stimuli were generated on a Power Macintosh G4 and were presented on a 19W LaCie Electron Blue II CRT monitor (LaCie USA, Hillsboro, OR). Both Vernier and lateral motion stimuli subtended 29° × 22° at a viewing distance of 70 cm. The grating stimuli subtended 13° × 10° at a viewing distance of 154 cm to yield the highest spatial frequency of 30 cpd (1 arcmin) used in this study. Participants were instructed to fixate on a mark at the center of the display and to distribute attention evenly over the entire display. The stimuli were viewed binocularly in a dark and quiet room.

## EEG data acquisition

To collect EEG data, 128-channel HydroCel "Sensor Nets" (Electrical Geodesics, Eugene, OR) were used.

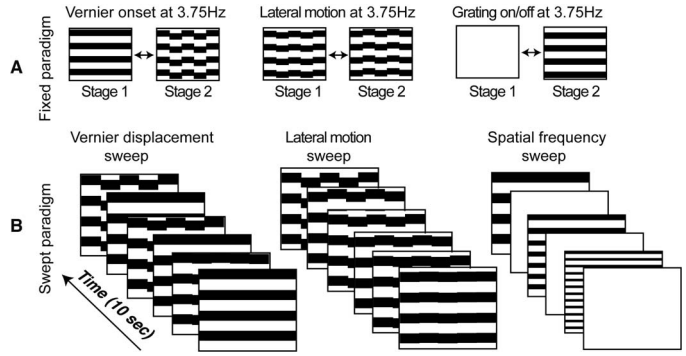


Figure 1. Schematic illustration of the stimuli used in SSVEP. Fixed paradigm (A) and swept paradigm (B) for Vernier onset/offset (left panel), lateral motion control (middle panel), and grating on/off (right panel) conditions, respectively. In each condition, the stimulus alternated between the two depicted states at 3.75 Hz. (A) In the Vernier onset/offset condition, 2 cpd square-wave gratings had alternate columns of Vernier displacements of 8 arcmin. In the lateral motion condition, successive frames had Vernier offsets in opposite directions with 4 arcmin offset in each direction to produce in total of 8 arcmin motion. Thus, the motion displacement in successive panels was the same in both conditions. The grating on/off condition had a 3 cpd sinusoidal grating (depicted as a square wave) that alternated between on and off (blank screen). (B) Corresponding sweep paradigms in which the value of the swept parameter changed over a period of 10 s. The size of the displacements of Vernier offset ranged from 0.5 to 8 arcmin in 10 equal logarithmic steps, and the spatial frequency of gratings ranged from 30 to 2 cpd in 10 equal linear steps.

Signals were 50 Hz low-pass and 0.1 Hz high-pass filtered and digitized at 500 Hz. At the end of the EEG session, three major fiducials (nasion, left and right periauricular points) and three-dimensional (3D) locations of all electrodes were digitized using a 3Space Fastrack 3D digitizer (Polhemus, Colchester, VT). These 3D locations were used to co-register the electrodes to the T1-weighted anatomical MRI scans. EEG raw data and artifact rejection, including blink rejection and eye movement artifact detection, were evaluated offline based on a sample-by-sample thresholding procedure using the software package designed by the Norcia research group (Ales, Appelbaum, Cottereau, & Norcia, 2013; Cottereau, Ales, & Norcia, 2015). Noisy sensors were replaced by the average of the six nearest spatial neighbors. The EEG was re-referenced to the common average of all the sensors after noisy sensors were substituted.

## Structural and functional MRI and visual area definition

Each participant had structural and functional MRI scanning conducted on a 3T Tim Trio scanner (Siemens, Munich, Germany) using a 12-channel head coil in a separate session. We acquired a T1-weighted MRI data set (3-D MP-RAGE sequence, $0.8 \times 0.8 \times 0.8$ mm$^3$) and a 3D T2- weighted data set (spin echo sequence at $1 \times 1 \times 1$ mm$^3$ resolution) for tissue segmentation and registration with the functional scans. For the fMRI, we used a single-shot, gradient-echo EPI sequence (TR/TE, 2,000/28 ms; flip angle, 80°; 126 volumes per run) with a voxel size of $1.7 \times 1.7 \times 2$ mm$^3$ ($128 \times 128$ acquisition matrix; 220 mm field of view; bandwidth, 1860 Hz/pixel; echo spacing, 0.71 ms). We acquired 30 slices without gaps, positioned between the coronal and axial planes, roughly tangent to the cortical surface near the parieto-occipital sulci at the midline, which maximized cerebral coverage at the expense of the cerebellum.

The FreeSurfer software package (http://surfer.nmr.mgh.harvard.edu) was used to perform gray and white matter segmentation and extraction of the mid-gray cortical surface used for source locations. We made separate models for each observer using the boundary element method, with boundary surfaces derived from the T1- and T2-weighted MRI scans of each observer (Jenkinson, Pechaud, & Smith, 2005; Smith, 2002) using the FMRIB Software Library (http://fsl.fmrib.ox.ac.uk/fsl/). Forward and inverse electrical models were made with MNE (http://martinos.org/mne/stable/index.html) using a standard set of conductances (0.33, 0.025, and 0.33 S/m for the scalp, skull, and brain compartment, respectively).

Retinotopic regions of interest (ROIs) corresponding to areas in early visual cortical areas V1, V2v, V2d, V3v, V3d, V3a, and hV4 in each hemisphere (Engel, Glover, & Wandell, 1997; Huk & Heeger, 2002; Press, Brewer, Dougherty, Wade, & Wandell, 2001; Sereno et al., 1995; Tootell et al., 1997; Wade, Brewer, Rieger, & Wandell, 2002) were mapped using rotating wedges and expanding rings of contrast-reversing checkerboards (Brewer, Liu, Wade, & Wandell, 2005). ROIs corresponding to hMT+ were identified using low-contrast motion stimuli similar to those described by Huk and Heeger (2002). The lateral occipital cortex (LOC) was defined using a block-design fMRI localizer scan with stimuli from Kourtzi and Kanwisher (2000).

## Cortically constrained inverse

L2 minimum norm inverse was computed with sources constrained to the location and orientation of the cortical surface (Hämäläinen, Hari, Ilmoniemi, Knuutila, & Lounasmaa, 1993). We also modified the source covariance matrix to decrease the tendency of the minimum norm procedure to place sources outside of visual areas. These constraints involved (a) increasing the variance allowed within the visual areas by a

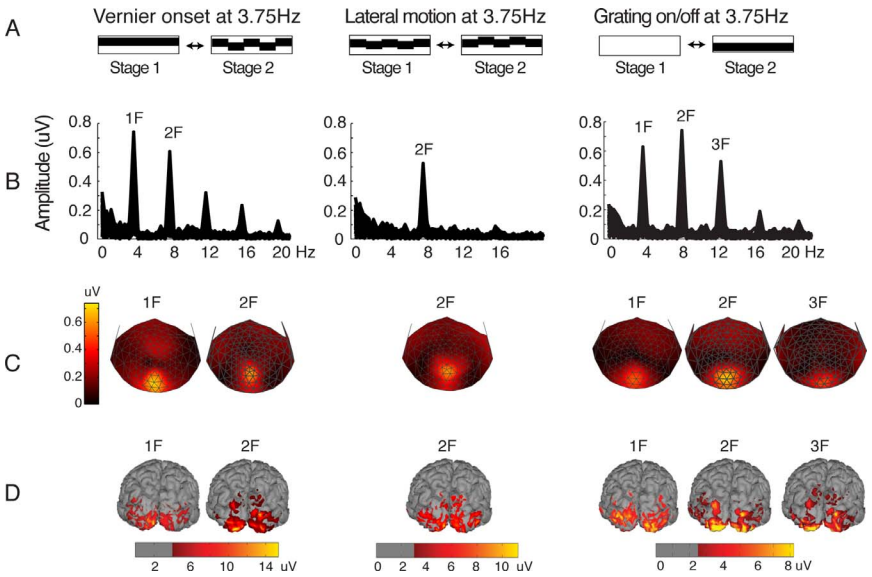


Figure 2. Evoked responses to different stimuli at 3.75 Hz. (A) Illustration of fixed paradigm VEP stimuli. (Left) Vernier onset/offset of a square-wave grating. (Middle) Lateral motion. (Right) Sine-wave grating on/off. (B) Fourier spectrum for the responses to the stimuli in A: The spectrum is the average activity of participants across 128 electrodes. Topological scalp activities (C) and surface-based cortical source activities viewed from behind (D) averaged from all participants for Vernier onset/offset at first two harmonics (1F, 2F), for lateral motion control at the second harmonic (2F), and for grating on/off at the first three harmonics (1F, 2F, and 3F). Activities of cortical sources at specific harmonic components in D were mapped from all participants to one participant's cortex.

factor of two relative to other vertices and (b) enforcing a local smoothness constraint within an area using the first- and second-order neighborhoods on the mesh with a weighting function equal to 0.5 for the first order and 0.25 for the second, which greatly increases the confidence in our estimates of source activity (for review, see Cottereau et al., 2015).

## Cross-talk in the ROIs

We are interested in all visual cortical areas including V1, V2v, V2d, V3v, V3d, V3a, hV4, LOC, and hMT+ and investigate their sensitivities to Vernier acuity and grating acuity. However, the smoothing of the electric field by the head volume might result in cross talk among visual ROIs obtained with our inverse approach. *Cross-talk* refers to the neural signals measured in a particular ROI due to activity generated in a different ROI. Thus, before performing ROI-based analysis, we evaluated the global cross-talk matrix using the calculation described in Lauritzen, Ales, and Wade (2010). Ideally, the cortical current densities between ROIs would show zero cross-talk and the associated matrix would be equal to the identity matrix, but the skull, dura, and intervening media smear our source localization. Our calculation showed that visual areas V1, hV4, LOC, and hMT+ received on average less than 20% cross-talk from other areas, allowing us to conclude that the results we observed arise predominantly in these areas. However, V2 and V3 had significant cross-talk from other areas. These ROIs were therefore excluded from our analysis.

## ROI-based analysis of the SSVEP

In the current study, we specifically looked at the ROIs in V1, hV4, LOC, and hMT+. The EEG recording session consisted of 10 trials per condition for all participants. For each participant and stimulus condition, channel and raw EEG recordings for each 10-s trial were partitioned into 10 sequential epochs. For the fixed-paradigm stimuli, these epochs were averaged together within each trial and then across trials to obtain a single grand average waveform for each participant, channel, and stimulus condition. Each grand average waveform was Fourier transformed and digitally filtered with a low-pass filter with a cutoff of 50 Hz to remove 60 Hz and other high-frequency noise. A new waveform corresponding to a single stimulus cycle (267-ms duration, or 3.75 Hz) was then reconstructed by inverse Fourier transformation of this filtered spectrum. These reconstructed waveforms were then averaged together across participants for each ROI and stimulus condition. We also analyzed the first (1F) and second (2F) harmonic component of the stimulus-driven frequencies (3.75 Hz). The responses at 1F and 2F were coherently averaged in each ROI across the

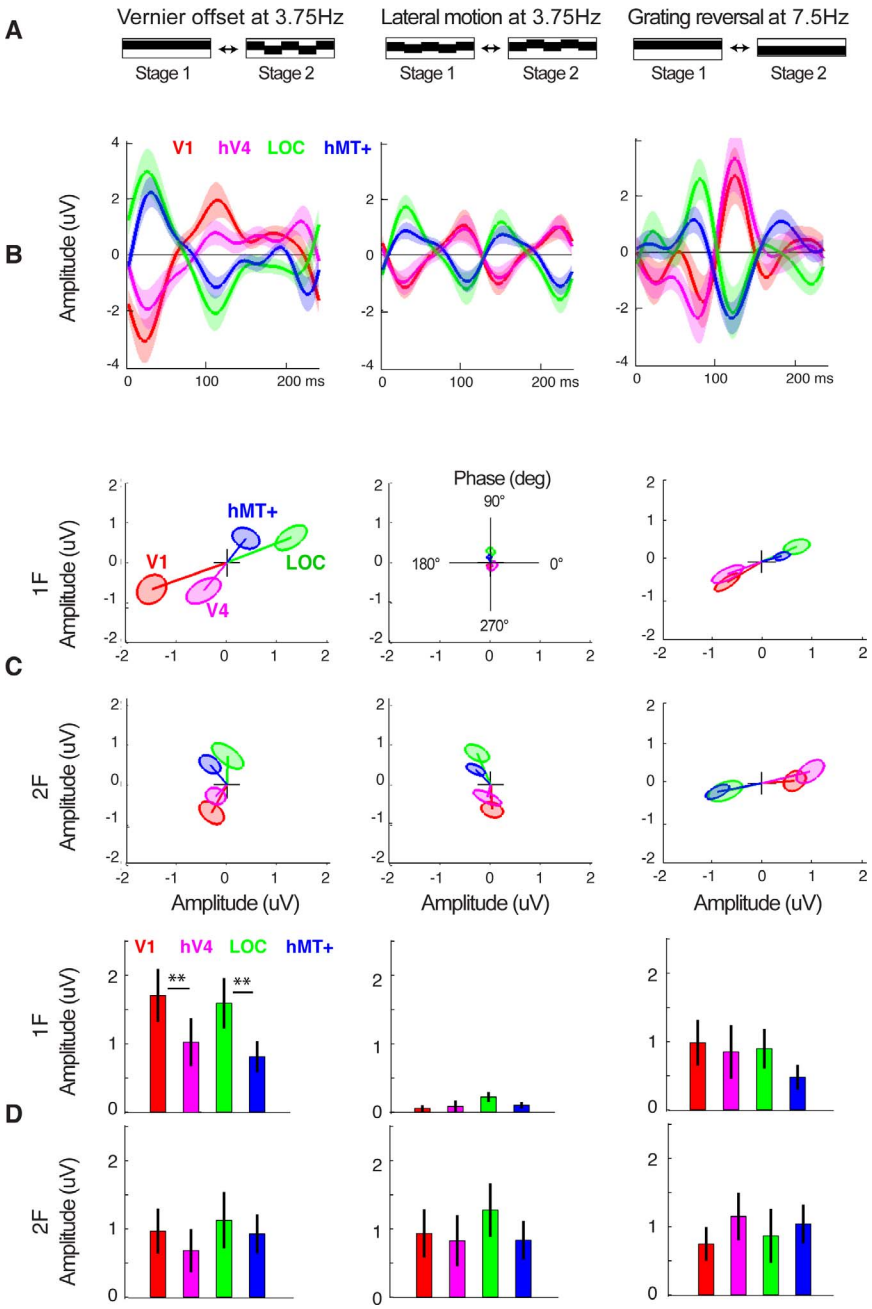


Figure 3. ROI-based responses to Vernier, motion, and grating stimuli. (A) Illustration of the stimuli. (B) Averaged time courses of the responses to Vernier onset/offset (left panel), motion control (middle panel), and grating on/off (right panel) stimuli in visual ROIs. Data have been further filtered to remove frequencies greater than 20 Hz for ease of visualization. The shaded areas around the waveforms correspond to the standard errors. (C) Two-dimensional amplitude and phase responses along with standard errors in different ROIs are shown for 1F (top row) and 2F (bottom row). (D) Response amplitudes in different ROIs averaged coherently from all participants. $^{**}p < 0.01$.

participants (Figure 3D). In the swept paradigm stimuli, to measure the response functions, raw EEG recordings for each 10-s trial were divided into 10 sequential epochs that corresponded to the swept stimulus values. For each epoch, a recursive least-square adaptive filter (Tang & Norcia, 1995) was used to generate a series of complex-valued spectral coefficients representing the amplitude and phase of response components (harmonics, e.g., 1F and 2F; Hou et al., 2007). Voltage versus displacement/spatial frequency functions were obtained by coherently averaging the spectral coefficients for each epoch across trials for each participant, ROI, harmonic, and stimulus condition (Figures 4 and 5).

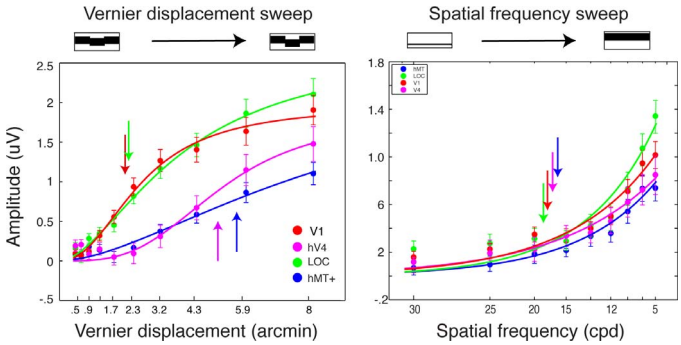


Figure 4. ROI-based first harmonic responses from sweep paradigm. SSVEP responses averaged across participants as a function of Vernier displacement (left panel) and spatial frequency (right panel). The colors represent cortical areas V1 (red), hV4 (purple), LOC (green), and hMT+ (blue). The solid lines represent the first harmonic responses fit by a generalized Naka-Rushton equation (see the Methods section and text). The arrows point to the semisaturation constant (response threshold) in each ROI.

## Statistical analysis

The phase differences in Figure 3C were analyzed using a circular statistics toolbox (CircStat; Berens, 2009). Specifically, the Watson-Williams test (Watson & Williams, 1956) was used for phase differences between ROIs (Table 1).The standard analysis of variance (ANOVA) in Figure 3D, Figure 4, and Figure 5 used a within-subject design and was conducted. We used two-tailed paired $t$ tests for the data in Figure 4 (Table 3) and Figure 5 (Table 4). Bonferroni correction was used to control the familywise error rate for repeated, paired tests in four ROIs, with an adjusted significance level of $0.05/4 = 0.0125$.

In Figures 4 and 5, a generalized Naka-Rushton equation, $y = ax^n/(x^n + b^n)$, was used to fit the response functions of both Vernier displacement and spatial frequency, where $a$ is the maximum amplitude, $b$ is the semisaturation constant, and $n$ is the exponent.

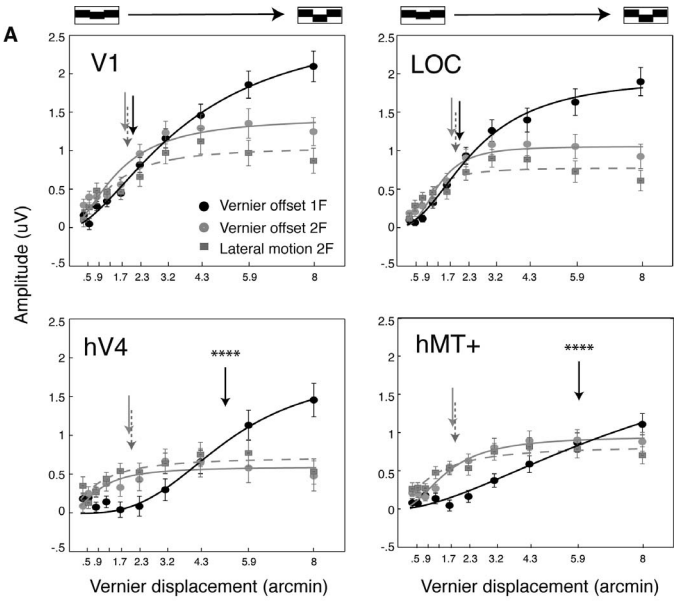


Figure 5. Comparison of sensitivity to relative position and motion in each ROI. SSVEP responses averaged across 15 participants as a function of Vernier displacement and lateral motion in different ROIs. The solid lines represent the first and second harmonic responses for Vernier onset/offset stimuli, and the dashed lines represent the second harmonic responses for lateral motion control stimuli. Both solid and dashed lines are fit by a generalized Naka-Rushton equation (see the Methods section and text). The arrows point to the semisaturation constant in each ROI. ****Paired $t$ test between 1F and 2F of the Vernier response is significant at $p < 0.0001$.

# Results

## Brain activities evoked by suprathreshold Vernier displacements and gratings

Response spectra for the Vernier onset/offset, motion control, and grating on/off stimuli are shown in Figure 2B. The spectrum across the 128 electrodes is

| | Phase in ROIs ($M \pm SD$, °) | | | | $p$ | | | | | |
|---|---|---|---|---|---|---|---|---|---|---|
| | V1 | hV4 | LOC | hMT+ | V1 vs. hV4 | LOC vs. hMT+ | V1 vs. LOC | hV4 vs. hMT+ | V1 vs. hMT+ | LOC vs. hV4 |
| 1F | | | | | | | | | | |
| Vernier | −93 ± 124 | −67 ± 94 | 87 ± 119 | 149 ± 122 | 0.029 | 0.228 | <0.0001 | <0.0001 | <0.0001 | <0.0001 |
| Grating | −120 ± 68 | −46 ± 129 | 143 ± 135 | 145 ± 143 | 0.334 | 0.846 | <0.0001 | <0.0001 | <0.0001 | <0.0001 |
| 2F | | | | | | | | | | |
| Vernier | −64 ± 94 | −18 ± 112 | 134 ± 94 | 168 ± 91 | 0.869 | 0.329 | <0.0001 | 0.0005 | <0.0001 | 0.0001 |
| Motion | −58 ± 82 | −56 ± 114 | 78 ± 82 | 100 ± 69 | 0.238 | 0.519 | <0.0001 | 0.0007 | <0.0001 | <0.0001 |
| Grating | 22 ± 77 | −8 ± 82 | 166 ± 70 | 197 ± 90 | 0.685 | 0.757 | <0.0001 | 0.0002 | 0.0036 | 0.0003 |

Table 1. Response phases in ROIs and Watson-Williams test between ROIs. *Notes*: The 1F for motion control condition did not produce significant responses and is therefore not included. Adjusted significance level with Bonferroni correction is 0.0125.

| | | ROIs ($M \pm SD$ of fit parameters) | | | | ANOVA results | | |
|---|---|---|---|---|---|---|---|---|
| Measure | Fit | V1 | hV4 | LOC | hMT+ | $F$ | $df$ | $p$ |
| Vernier | $a$ | 2.27 ± 1.83 | 2.73 ± 1.68 | 2.38 ± 1.35 | 2.21 ± 1.2 | 0.87 | 3, 12 | 0.483 |
| | $b$ | 2.02 ± 0.6 | 4.58 ± 1.78 | 2.35 ± 0.8 | 5.83 ± 1.75 | 37.3 | 3, 12 | **<0.0001** |
| | $n$ | 2.21 ± 0.8 | 1.51 ± 0.88 | 1.73 ± 0.79 | 1.7 ± 0.8 | 1.8 | 3, 12 | 0.201 |
| Grating | $a$ | 2.82 ± 1.64 | 2.56 ± 2.03 | 2.78 ± 1.45 | 1.82 ± 1.13 | 1.28 | 3, 9 | 0.339 |
| | $b$ | 17.24 ± 4.37 | 18.07 ± 2.88 | 18.45 ± 3.83 | 17.4 ± 4.63 | 1.14 | 3, 9 | 0.384 |
| | $n$ | −4.12 ± 2.02 | −4.25 ± 1.78 | −4.61 ± 1.94 | −3.71 ± 1.41 | 0.74 | 3, 9 | 0.557 |

Table 2. One-way ANOVA results for each fit parameter of the Vernier and grating responses. Bold font represents a significant $p$-value.

overlaid, where each electrode is a sensor-by-sensor average across all participants. Consistent with previous studies that used a similar stimulus paradigm (Amoore et al., 2008; Chen, Norcia, Pettet, & Chandna, 2005; Hou et al., 2007; Norcia et al., 1999; Skoczenski & Norcia, 1999), the suprathreshold Vernier onset/offset stimulus in our study produced responses predominantly at the first harmonic (1F) and second harmonic (2F) components of the stimulus frequency, whereas the motion-control condition produced only a 2F response. The grating on/off stimuli, which had the same temporal frequency as the Vernier onset/offset stimuli, produced responses dominated by the first (1F), second (2F), and third (3F) harmonic components (Hou, Good, & Norcia, 2015).

Topological scalp activities and associated surface-based cortical activities averaged across all participants are shown in Figure 2C and Figure 2D, respectively. The cortical surface (Figure 2D) is presented from behind to focus on the activated regions. Both topological scalp and cortical surfaces show that the predominant response harmonics to Vernier onset/offset, lateral motion, and grating on/off stimuli were in the occipital and lateraloccipital areas (Figure 2C, D).

| ROIs ($M \pm SD$) | |
|---|---|
| V1 | 2.02 ± 0.6 |
| hV4 | 4.58 ± 1.78 |
| LOC | 2.35 ± 0.8 |
| hMT+ | 5.83 ± 1.75 |
| $p$ | |
| V1 vs. hV4 | **<0.0001** |
| LOC vs. hMT+ | **<0.0001** |
| V1 vs. LOC | 0.044 |
| hV4 vs. hMT+ | 0.0914 |
| V1 vs. hMT+ | **<0.0001** |
| LOC vs. hV4 | **0.0003** |

Table 3. Paired $t$ tests for semisaturation constant ($b$) value of Vernier response between ROIs. *Notes*: Adjusted significance level with Bonferroni correction is 0.0125. Bold font represents a significant $p$-value.

## ROI-based analysis for suprathreshold Vernier and grating stimuli

Figure 3B shows the time course of responses averaged across all participants to three fixed stimuli (8 arcmin Vernier onset/offset, 8 arcmin lateral motion control, and 3 cpd grating on/off) in the visual ROIs. The responses at V1 and hV4 are phase shifted by about 180° from the responses at LOC and hMT+ for all three stimuli. This phase shift can be seen also at the predominant harmonic components for each stimulus (Figure 3C). The phase shift by about 180° between V1/hV4 and LOC/hMT+ is likely due to the anatomical structure of these visual areas, as a similar phase shift was also found in other study with different stimuli (Cottereau, McKee, Ales, & Norcia, 2011). To further confirm whether response phases were significantly different among ROIs as seen in Figure 3C, multiple Watson-Williams tests were conducted for each stimulus and each harmonic component, and the results are shown in Table 1.

Figure 3D plots the response amplitudes for different stimuli at the 1F (upper row) and the 2F (lower row) harmonics, averaged coherently across all participants. We conducted within-subjects two-way ANOVA separately for 1F and 2F because the two harmonic components reflect different mechanisms in Vernier onset/offset stimuli (Norcia et al., 1999). For the 1F analysis, we did not include the motion control stimuli because they did not generate a 1F response. Thus, Stimuli (2) × ROIs (4) ANOVA at 1F revealed an interaction of Stimuli and ROIs, $F(6, 7) = 4.36$, $p = 0.037$, $f = 4.36$. There was a significant main effect of ROIs for the Vernier onset/offset stimulus, $F(6, 9) = 4.29$, $p = 0.026$, $f = 4.29$, but there was not a significant main effect of ROIs for the grating stimulus, $F(6, 7) = 1.16$, $p = 0.420$, $f = 1.16$, revealed by the following one-way ANOVA. This result indicates that the Vernier stimulus evokes a different first harmonic response

| ROIs | Fit Harmonics | a | | b | | n | |
|---|---|---|---|---|---|---|---|
| | | M ± SD | p | M ± SD | p | M ± SD | p |
| V1 | 1F | 2.2 ± 1.77 | | 1.89 ± 0.64 | | 2.21 ± 0.8 | |
| | 2F | 1.59 ± 1.17 | | 1.45 ± 0.51 | | 2.3 ± 1.04 | |
| | 1F vs. 2F | | 0.0287 | | 0.033 | | 0.7251 |
| hV4 | 1F | 2.73 ± 1.68 | | 4.58 ± 1.78 | | 1.51 ± 0.88 | |
| | 2F | 1.6 ± 1.02 | | 1.6 ± 0.71 | | 1.99 ± 0.8 | |
| | 1F vs. 2F | | 0.0133 | | **<0.0001** | | 0.1478 |
| LOC | 1F | 2.38 ± 1.35 | | 2.35 ± 0.8 | | 1.73 ± 0.79 | |
| | 2F | 2.31 ± 1.34 | | 1.81 ± 0.48 | | 1.85 ± 0.78 | |
| | 1F vs. 2F | | 0.8304 | | 0.0382 | | 0.7148 |
| hMT+ | 1F | 2.21 ± 1.2 | | 5.83 ± 1.75 | | 1.7 ± 0.8 | |
| | 2F | 1.48 ± 0.79 | | 1.67 ± 0.72 | | 2.13 ± 1.39 | |
| | 1F vs. 2F | | 0.0248 | | **<0.0001** | | 0.2944 |

Table 4. Paired *t* tests for 1F and 2F harmonic components of Vernier offset stimuli. *Notes*: Adjusted significance level with Bonferroni correction is 0.0125. Bold font represents a significant *p*-value.

across ROIs compared with the grating stimulus. Because of data with complex harmonic coefficients, we cannot perform simple *t* tests between ROIs for the 1F component of the Vernier stimulus. Instead, one-way ANOVAs for two pairs of ROIs (V1 vs. hV4; LOC vs. hMT+) were conducted, because each of these pairs has the same response phase (see Figure 3C and Table 1). The statistical results indicated that V1 amplitude was stronger than that of hV4, $F(2, 13) = 8.74$, $p = 0.004$, $f = 8.74$, and that LOC amplitude was stronger than that of hMT+, $F(2, 13) = 6.81$, $p = 0.009$, $f = 6.81$.

For the 2F responses, Stimuli (3) × ROIs (4) ANOVA revealed no significant interaction of Stimuli and ROIs, $F(12, 1) = 4.13$, $p = 0.369$, $f = 4.13$, indicating no amplitude differences for the second harmonic responses for all three stimuli.

## Cortical sources of sensitivity to Vernier and grating acuity

In the first experiment, we demonstrated that suprathreshold Vernier stimuli (8 arcmin) elicited stronger 1F responses in visual areas V1 and LOC than in hV4 and hMT+, whereas suprathreshold grating stimuli (3 cpd) elicited similar 1F responses in all ROIs. In the next experiment, we swept stimulus parameters from subthreshold to suprathreshold values for all three stimuli to measure near-threshold responses.

Previous studies have demonstrated that Vernier displacement thresholds determined from 1F responses reflect Vernier acuity (Norcia et al., 1999), whereas the spatial frequency threshold at all harmonics of grating on/off responses reflect grating acuity (Hou et al., 2015; Tang & Norcia, 1995). Thus, we focused on the analysis of the 1F component. Figure 4 plots the 1F responses as a function of the swept parameters in different visual ROIs, averaged coherently across all participants. The data of one of 13 participants in the spatial frequency sweep paradigm were excluded because of low signal-to-noise ratio. The solid lines represent fits to the data of a generalized Naka-Rushton equation, $y = ax^n/(x^n + b^n)$, where $a$ is the maximum amplitude, $b$ is the semisaturation constant, and $n$ is the exponent. A separate one-way (ROIs) ANOVA for each fit parameter of the Vernier and grating response showed no significant difference, except for $b$ of Vernier stimuli ($p < 0.0001$; see Table 2). A further paired $t$ test of the Vernier semisaturation constant showed significantly lower values in V1 and LOC than in hMT+ and hV4 (with Bonferroni correction) but no significant difference between V1 and LOC or between hV4 and hMT+ (Table 3). Because the semisaturation constant ($b$) value reflects the sensitivities of the response functions, we define it as the "response threshold." The response threshold measure for detecting Vernier displacement indicates that cortical areas V1 and LOC are particularly sensitive to near-threshold Vernier displacements, whereas cortical areas hV4 and hMT+ are less sensitive. This sensitivity difference between ROIs to Vernier stimuli can be seen clearly in the left panel of Figure 4, where the arrows point to the semisaturation constant (response threshold) in each ROI. In contrast, all ROIs (V1, LOC, hV4, and hMT+) showed similar sensitivity to near-threshold spatial frequencies (see Figure 4, right panel).

## Cortical sources for sensitivity to relative position and motion

With a dedicated design, Norcia et al. (1999) demonstrated that the Vernier onset/offset paradigm that we use in the current study produces both 1F and

2F components that reflect different mechanisms: 1F for Vernier acuity and 2F for motion sensitivity. Therefore, to localize the cortical sources for sensitivity to relative position (Vernier acuity) and relative motion, we compared response functions of the 1F and 2F components in different ROIs (Figure 5). The 2F response functions of the motion control stimulus were also compared.

Consistent with the description of Norcia et al. (1999), the 2F response functions of the Vernier onset/offset and motion control stimuli were virtually identical, as seen in Figure 5. This was also confirmed by Fit (3) × Stimulus (2) × ROI (4) ANOVA, in which the main effect of stimulus was not significant, $F(1, 14) = 0.01$, $p = 0.914$, $f = 1.22$, and the interaction of Stimulus and Fit parameter was also not significant, $F(2, 13) = 1.95$, $p = 0.182$, $f = 1.95$.

Next, we focused on the Vernier onset/offset paradigm to compare the response functions between relative position (1F) and motion (2F) in each ROI. We first conducted Fit (3) × Harmonics (2) × ROIs (4) ANOVA, in which there were significant main effects of Fit, $F(2, 13) = 19.49$, $p < 0.001$, $f = 19.49$; Harmonics, $F(1, 14) = 28.86$, $p < 0.001$, $f = 28.86$; and ROIs, $F(3, 12) = 6.10$, $p = 0.009$, $f = 6.09$. The interaction of Fit, Harmonics, and ROIs was significant, $F(6, 9) = 21.22$, $p < 0.001$, $f = 21.22$. Then, further paired $t$ tests were performed for comparison of fit parameters for 1F and 2F in each ROI (Table 4). In V1 and LOC, there was no difference between 1F and 2F response thresholds (semisaturation constant, $b$), indicating that V1 and LOC are sensitive to both relative position (Vernier acuity) and relative motion. By contrast, the response thresholds for 1F and 2F in hV4 and hMT+ were significantly different, with lower thresholds for 2F than 1F, indicating that cortical areas hV4 and hMT+ are more sensitive to relative motion than relative position (Vernier acuity). The other fit parameters ($a$ and $n$) between 1F and 2F in all ROIs were not significant.

## Discussion

Using fMRI-informed EEG source imaging, we measured neural population responses to Vernier, grating, and motion stimuli at different stages of the visual cortical hierarchy in humans. Our results indicate that visual cortical areas, including V1 and extrastriate cortex (hV4, LOC, and hMT+), respond to supra- and near-threshold Vernier and grating stimuli as well as relative motion stimuli in characteristic patterns. Cortical areas V1 and LOC are particularly sensitive to the detection of Vernier displacement, whereas all visual ROIs (V1, hV4, LOC, and hMT+) are sensitive to relative motion. In contrast, near-threshold grating stimuli elicited similar responses in all visual ROIs.

We replicated previous VEP studies (Chen et al., 2005; Hou et al., 2007; Norcia et al., 1999) in which the Vernier onset/offset stimulus produced robust first and second harmonic responses, whereas the lateral motion control stimulus produced only second harmonic responses. Using source localization of EEG responses, we further identified the cortical sources of those harmonic components described by previous studies. Furthermore, our study reveals that some extrastriate areas are more sensitive to near-threshold Vernier displacements. For instance, we demonstrate that the LOC is as sensitive to Vernier displacements as V1 and much more sensitive than hV4 or hMT+, whereas all ROIs have the same sensitivities to motion stimuli. The high sensitivity of V1 to Vernier displacements provides strong evidence that it has a role in extracting hyperacuity information. This finding is in agreement with the assumption that striate mechanisms underlie Vernier acuity, proposed by a large body of computational models (Duncan & Boynton, 2003; Klein & Levi, 1985; Watt & Morgan, 1985; Wilson, 1986) and psychophysical studies (Findlay, 1973; Levi et al., 2000; Waugh et al., 1993).

It is also clear that LOC is as sensitive as V1 to Vernier displacements. The role of LOC in hyperacuity processing has not yet been documented. It is not clear whether area LOC simply inherits its sensitivity from V1 or whether it is specialized for hyperacuity related to texture segregation and object processing. Previous studies have shown that LOC is an object-related area and associated with the figure-ground segregation of textures (Appelbaum, Wade, Vildavski, Pettet, & Norcia, 2006; Grill-Spector, Kourtzi, & Kanwisher, 2001; Grill-Spector, Kushnir, Edelman, Itzchak, & Malach, 1998). It is possible that discontinuity of bars/lines (Vernier displacements) is similar to texture segmentation, which activates LOC (Appelbaum et al., 2006). It is also possible that LOC is highly responsive to the relative position of visual features, as it plays a key role in object recognition, which requires comparison of the relative position of features (Grill-Spector et al., 1998; Grill-Spector et al., 2001).

In contrast to Vernier acuity, our results show that the four visual areas we examined have similar detection thresholds for spatial frequency (grating acuity). This finding supports the general view that grating acuity, the resolution cutoff, is limited faithfully by retinal-striate factors, because it is in agreement with photoreceptor sampling limits in the retina (Levi et al., 1985). The striate cortex (V1), therefore, may faithfully pass the orientation-tuned resolution information from the retina on to extrastriate cortices without further

filtering, as seen by the similar sensitivities to spatial frequency at all ROIs.

The differing pattern of sensitivity to Vernier and grating across neural populations has important clinical implications. For example, discrepancies between Vernier and grating acuity measures in amblyopia have been reported for decades, with strabismic amblyopes showing more severe losses in Vernier acuity than in grating acuity (Birch & Swanson, 2000; Levi & Klein, 1982a, 1982b, 1985; Levi, Klein, & Wang, 1994a, 1994b; Levi, Klein, & Yap, 1987; McKee et al., 2003). This clinical discrepancy implies that grating acuity may not fully reveal amblyopic deficits because of its limitation to retinal-striate factors. By contrast, Vernier acuity may better represent amblyopic deficits, particularly in strabismic amblyopia, because of the involvement of both striate and extrastriate cortical areas in Vernier acuity. This conjecture is consistent with recent studies that report extrastriate function deficits in amblyopia, especially in strabismic amblyopia (Ho & Giaschi, 2006; Hou, Pettet, & Norcia, 2008, 2014; Simmers, Ledgeway, & Hess, 2005; Simmers, Ledgeway, Hess, & McGraw, 2003; Simmers, Ledgeway, Mansouri, Hutchinson, & Hess, 2006). Hou et al. (2014) reported that responses to stimuli that activate LOC were severely reduced in strabismic amblyopes as compared with anisometropic amblyopes. Therefore, Vernier acuity may faithfully represent the cortical deficits in amblyopia, especially in strabismic amblyopia.

In summary, source estimates from high-density EEG recordings show that both striate and extrastriate cortices are involved in Vernier acuity processing. V1 and LOC are particularly sensitive to the detection of Vernier displacements, whereas all visual ROIs are sensitive to relative motion. Our results support a role for V1 in Vernier acuity related to its exquisite sensitivity to orientation differences. The robust activation of LOC might be related to the sensitivity to the relative position of features, which is common to Vernier displacement and to some kinds of texture segmentation.

*Keywords: Vernier acuity, lateral occipital cortex, V1, EEG source imaging, grating acuity*

## Acknowledgments

This work was supported by National Institutes of Health Grant R01-EY025018 and The West China Hospital Fund to CH, grants from The Smith-Kettlewell Eye Research Institute and Pacific Vision Foundation to CH and PV, and an Institute for Basic Science Grant R001-D1 to YJK. We thank Spero Nicholas for conducting MRI scans and for assistance in data analysis and Margaret Q. McGovern for assistance in recruiting the participants. The authors declare no competing financial interests.

Commercial relationships: none.
Corresponding author: Chuan Hou.
Email: chuanhou@ski.org.
Address: 2318 Fillmore Street, San Francisco, CA 94115, USA.

## References

Ales, J. M., Appelbaum, L. G., Cottereau, B. R., & Norcia, A. M. (2013). The time course of shape discrimination in the human brain. *Neuroimage*, *67*, 77–88.

Amoore, J. N., Lemesre, Y., Murray, I. C., Mieke, S., King, S. T., Smith, F. E., & Murray, A. (2008). Automatic blood pressure measurement: the oscillometric waveform shape is a potential contributor to differences between oscillometric and auscultatory pressure measurements. *Journal of Hypertension*, *26*, 35–43.

Appelbaum, L. G., Wade, A. R., Vildavski, V. Y., Pettet, M. W., & Norcia, A. M. (2006). Cue-invariant networks for figure and background processing in human visual cortex. *Journal of Neuroscience*, *26*, 11695–11708.

Berens, P. (2009). CircStat: A MATLAB toolbox for circular statistics. *Journal of Statistical Software*, *31*(10), 121.

Birch, E. E., & Swanson, W. H. (2000). Hyperacuity deficits in anisometropic and strabismic amblyopes with known ages of onset. *Vision Research*, *40*, 1035–1040.

Brewer, A. A., Liu, J., Wade, A. R., & Wandell, B. A. (2005). Visual field maps and stimulus selectivity in human ventral occipital cortex. *Nature Neuroscience*, *8*, 1102–1109.

Chen, S. I., Norcia, A. M., Pettet, M. W., & Chandna, A. (2005). Measurement of position acuity in strabismus and amblyopia: specificity of the Vernier VEP paradigm. *Investigative Ophthalmology & Visual Science*, *46*, 4563–4570. [PubMed] [Article]

Cottereau, B. R., Ales, J. M., & Norcia, A. M. (2015). How to use fMRI functional localizers to improve EEG/MEG source estimation. *Journal of Neuroscience Methods*, *250*, 64–73.

Cottereau, B. R., McKee, S. P., Ales, J. M., & Norcia, A. M. (2011). Disparity-tuned population responses from human visual cortex. *Journal of Neuroscience*, *31*, 954–965.

Duncan, R. O., & Boynton, G. M. (2003). Cortical magnification within human primary visual cortex correlates with acuity thresholds. *Neuron*, *38*, 659–671.

Engel, S. A., Glover, G. H., & Wandell, B. A. (1997). Retinotopic organization in human visual cortex and the spatial precision of functional MRI. *Cerebral Cortex*, *7*, 181–192.

Findlay, J. M. (1973). Feature detectors and Vernier acuity. *Nature*, *241*, 135–137.

Geisler, W. S. (1984). Physical limits of acuity and hyperacuity. *Journal of the Optical Society of America A*, *1*, 775–782.

Grill-Spector, K., Kourtzi, Z., & Kanwisher, N. (2001). The lateral occipital complex and its role in object recognition. *Vision Research*, *41*, 1409–1422.

Grill-Spector, K., Kushnir, T., Edelman, S., Itzchak, Y., & Malach, R. (1998). Cue-invariant activation in object-related areas of the human occipital lobe. *Neuron*, *21*, 191–202.

Hämäläinen, M., Hari, R., Ilmoniemi, R., Knuutila, J., & Lounasmaa, O. V. (1993). Magnetoencephalography: Theory, instrumentation and applications to the noninvasive study of human brain function. *Reviews of Modern Physics*, *65*, 413–497.

Ho, C. S., & Giaschi, D. E. (2006). Deficient maximum motion displacement in amblyopia. *Vision Research*, *46*, 4595–4603.

Hou, C., Good, W. V., & Norcia, A. M. (2007). Validation study of VEP Vernier acuity in normal-vision and amblyopic adults. *Investigative Ophthalmology & Visual Science*, *48*, 4070–4078. [PubMed] [Article]

Hou, C., Good, W. V., & Norcia, A. (2015). Detection of amblyopia using sweep VEP grating and Vernier acuity. *Investigative Ophthalmology & Visual Science*, *56*, 2202.

Hou, C., Pettet, M. W., & Norcia, A. M. (2008). Abnormalities of coherent motion processing in strabismic amblyopia: Visual-evoked potential measurements. *Journal of Vision*, *8*(4):2, 1–12, doi: 10.1167/8.4.2. [PubMed] [Article]

Hou, C., Pettet, M. W., & Norcia, A. M. (2014). Acuity-independent effects of visual deprivation on human visual cortex. *Proceedings of the National Academy of Science, USA*, *111*, E3120–E3128.

Hubel, D. H., & Wiesel, T. N. (1962). Receptive fields, binocular interaction and functional architecture in the cat's visual cortex. *Journal of Physiology*, *160*, 106–154.

Huk, A. C., & Heeger, D. J. (2002). Pattern-motion responses in human visual cortex. *Nature Neuroscience*, *5*, 72–75.

Jenkinson, M., Pechaud, M., & Smith, S. (2005). BET2: MR-based estimation of brain, skull and scalp surfaces. In *Eleventh annual meeting of the organization for human brain mapping*. Oxford, UK: Oxford Centre for Functional Magnetic Resonance Imaging of the Brain (FMRIB).

Klein, S. A., & Levi, D. M. (1985). Hyperacuity thresholds of 1 sec: Theoretical predictions and empirical validation. *Journal of the Optical Society of America A*, *2*, 1170–1190.

Kourtzi, Z., & Kanwisher, N. (2000). Cortical regions involved in perceiving object shape. *Journal of Neuroscience*, *20*, 3310–3318.

Lauritzen, T. Z., Ales, J. M., & Wade, A. R. (2010). The effects of visuospatial attention measured across visual cortex using source-imaged, steady-state EEG. *Journal of Vision*, *10*(14):39, 1–17, doi: 10.1167/10.14.39. [PubMed] [Article]

Levi, D. M., & Klein, S. (1982a). Differences in Vernier discrimination for grating between strabismic and anisometropic amblyopes. *Investigative Ophthalmology & Visual Science*, *23*, 398–407. [PubMed] [Article]

Levi, D. M., & Klein, S. (1982b). Hyperacuity and amblyopia. *Nature*, *298*, 268–270.

Levi, D. M., & Klein, S. A. (1985). Vernier acuity, crowding and amblyopia. *Vision Research*, *25*, 979–991.

Levi, D. M., Klein, S. A., & Aitsebaomo, A. P. (1985). Vernier acuity, crowding and cortical magnification. *Vision Research*, *25*, 963–977.

Levi, D. M., Klein, S. A., & Carney, T. (2000). Unmasking the mechanisms for Vernier acuity: Evidence for a template model for Vernier acuity. *Vision Research*, *40*, 951–972.

Levi, D. M., Klein, S. A., & Wang, H. (1994a). Amblyopic and peripheral Vernier acuity: A test-pedestal approach. *Vision Research*, *34*, 3265–3292.

Levi, D. M., Klein, S. A., & Wang, H. (1994b). Discrimination of position and contrast in amblyopic and peripheral vision. *Vision Research*, *34*, 3293–3313.

Levi, D. M., Klein, S. A., & Yap, Y. L. (1987). Positional uncertainty in peripheral and amblyopic vision. *Vision Research*, *27*, 581–597.

Levi, D. M., Manny, R. E., Klein, S. A., & Steinman, S. B. (1983). Electrophysiological correlates of hyperacuity in the human visual cortex. *Nature*, *306*, 468–470.

McKee, S. P., Levi, D. M., & Movshon, J. A. (2003).

The pattern of visual deficits in amblyopia. *Journal of Vision*, *3*(5):5, 380–405, doi:10.1167/3.5.5. [PubMed] [Article]

Norcia, A. M., & Tyler, C. W. (1985). Spatial frequency sweep VEP: Visual acuity during the first year of life. *Vision Research*, *25*, 1399–1408.

Norcia, A. M., Wesemann, W., & Manny, R. E. (1999). Electrophysiological correlates of Vernier and relative motion mechanisms in human visual cortex. *Visual Neuroscience*, *16*, 1123–1131.

Press, W. A., Brewer, A. A., Dougherty, R. F., Wade, A. R., & Wandell, B. A. (2001). Visual areas and spatial summation in human visual cortex. *Vision Research*, *41*, 1321–1332.

Sereno, M. I., Dale, A. M., Reppas, J. B., Kwong, K. K., Belliveau, J. W., Brady, T. J., ... Tootell, R. B. (1995). Borders of multiple visual areas in humans revealed by functional magnetic resonance imaging. *Science*, *268*, 889–893.

Shapley, R., Hawken, M., & Ringach, D. L. (2003). Dynamics of orientation selectivity in the primary visual cortex and the importance of cortical inhibition. *Neuron*, *38*, 689–699.

Sheth, K. N., Walker, B. M., Modestino, E. J., Miki, A., Terhune, K. P., Francis, E. L., ... Liu, G. T. (2007). Neural correlate of Vernier acuity tasks assessed by functional MRI (FMRI). *Current Eye Research*, *32*, 717–728.

Simmers, A. J., Ledgeway, T., & Hess, R. F. (2005). The influences of visibility and anomalous integration processes on the perception of global spatial form versus motion in human amblyopia. *Vision Research*, *45*, 449–460.

Simmers, A. J., Ledgeway, T., Hess, R. F., & McGraw, P. V. (2003). Deficits to global motion processing in human amblyopia. *Vision Research*, *43*, 729–738.

Simmers, A. J., Ledgeway, T., Mansouri, B., Hutchinson, C. V., & Hess, R. F. (2006). The extent of the dorsal extra-striate deficit in amblyopia. *Vision Research*, *46*, 2571–2580.

Skoczenski, A. M., & Norcia, A. M. (1999). Development of VEP Vernier acuity and grating acuity in human infants. *Investigative Ophthalmology & Visual Science*, *40*, 2411–2417. [PubMed] [Article]

Skoczenski, A. M., & Norcia, A. M. (2002). Late maturation of visual hyperacuity. *Psychological Science*, *13*, 537–541.

Smith, S. M. (2002). Fast robust automated brain extraction. *Human Brain Mapping*, *17*, 143–155.

Srebro, R., & Osetinsky, M. V. (1987). The localization of cortical activity evoked by Vernier offset. *Vision Research*, *27*, 1387–1390.

Steinman, S. B., & Levi, D. M. (1992). Topography of the evoked potential to spatial localization cues. *Visual Neuroscience*, *8*, 281–294.

Steinman, S. B., Levi, D. M., Klein, S. A., & Manny, R. E. (1985). Selectivity of the evoked potential for Vernier offset. *Vision Research*, *25*, 951–961.

Tang, Y., & Norcia, A. M. (1995). An adaptive filter for steady-state evoked responses. *Electroencephalography and Clinical Neurophysiology*, *96*, 268–277.

Tootell, R. B., Mendola, J. D., Hadjikhani, N. K., Ledden, P. J., Liu, A. K., Reppas, J. B., ... Dale, A. M. (1997). Functional analysis of V3A and related areas in human visual cortex. *Journal of Neuroscience*, *17*, 7060–7078.

Victor, J. D., & Conte, M. M. (2000). Two-frequency analysis of interactions elicited by Vernier stimuli. *Visual Neuroscience*, *17*, 959–973.

Wade, A. R., Brewer, A. A., Rieger, J. W., & Wandell, B. A. (2002). Functional measurements of human ventral occipital cortex: retinotopy and colour. *Philosophical Transactions of the Royal Society B: Biological Sciences*, *357*, 963–973.

Watson, G., & Williams, E. (1956). On the construction of significance tests on the circle and the sphere. *Biometrika*, *43*, 344–352.

Watt, R. J., & Morgan, M. J. (1985). A theory of the primitive spatial code in human vision. *Vision Research*, *25*, 1661–1674.

Waugh, S. J., Levi, D. M., & Carney, T. (1993). Orientation, masking, and Vernier acuity for line targets. *Vision Research*, *33*, 1619–1638.

Westheimer, G. (1979). The spatial sense of the eye. Proctor lecture. *Investigative Ophthalmology & Visual Science*, *18*, 893–912. [PubMed] [Article]

Westheimer, G., & Hauske, G. (1975). Temporal and spatial interference with Vernier acuity. *Vision Research*, *15*, 1137–1141.

Wilson, H. R. (1986). Responses of spatial mechanisms can explain hyperacuity. *Vision Research*, *26*, 453–469.

Zak, R., & Berkley, M. A. (1986). Evoked potentials elicited by brief Vernier offsets: Estimating Vernier thresholds and properties of the neural substrate. *Vision Research*, *26*, 439–451.

Zemon, V., & Ratliff, F. (1982). Visual evoked potentials: Evidence for lateral interactions. *Proceedings of the National Academy of Sciences, USA*, *79*, 5723–5726.

Zemon, V., & Ratliff, F. (1984). Intermodulation components of the visual evoked potential: Responses to lateral and superimposed stimuli. *Biological Cybernetics*, *50*, 401–408.